https://www.scirp.org/journal/ns Natural Science, 2022, Vol. 14, (No. 6), pp: 251-263

Potential Power of the Pyramidal Structure VI: Pyramid Effects due to Potential Power and Pyramid Effects due to Bio-Entanglement

Osamu Takagi[1], Masamichi Sakamoto[2], Kimiko Kawano[1], Mikio Yamamoto[1]

[1]International Research Institute (IRI), Chiba, Japan; [2]Aquavision Academy, Chiba, Japan

Correspondence to: Osamu Takagi, takagi@a-iri.org

Keywords: Pyramid, Potential Power, Entanglement, Biosensor, *Cucumis sativus*, Gas, Psi Index

Received: June 4, 2022 **Accepted:** June 26, 2022 **Published:** June 29, 2022

ABSTRACT

Research on the so-called "pyramid power" began in the late 1930s. However, in general, pyramid power has been regarded as having no scientific basis, so there are very few systematic papers on pyramid power other than our academic research papers. Since October 2007, we have been conducting research to experimentally elucidate the unexplained phenomenon of a pyramid by using a pyramidal structure (PS). There have been two main types of experiments: (i) an experiment to detect the pyramid effects that appear due to the potential power (pyramid power) that the PS inherently has; and (ii) an experiment to detect the pyramid effects that appear when a test subject meditates inside the PS. To detect the pyramid effects, biosensors with evenly cut cucumber fruits, *Cucumis sativus*, were used. As a result of analyzing the concentration of volatile components emitted from the biosensors, we demonstrated the existence of pyramid power near the PS apex and discovered that the PS has the function of converting the unexplained energy of the meditator test subject. The research results so far have been reported as eleven original papers, three comprehensive reports, and one book chapter. We reported the phenomenon of the entanglement between biosensors in parts IV and V of the paper series, "Potential Power of the Pyramidal Structure". Furthermore, we clarified that the influence of the entanglement is included in the psi index Ψ, which is an index of the magnitude of the pyramid effects. The purpose of the present paper was to separate and analyze the psi index Ψ into the effect of the potential power of the PS and the effect of the entanglement between biosensors (we have named this as the Bio-Entanglement). To do this, we placed biosensors at the PS apex in two layers. The value of the pyramid effect on the biosensors in the upper layer was always larger than that in the lower layer. We found that this was mainly due to the potential power of the PS. We also found that the factor that caused the pyramid effect to change seasonally was mainly the

effect of the Bio-Entanglement. In short, we determined that the potential power of the PS, and the Bio-Entanglement had different effects on the biosensors. We were also able to propose a model that could qualitatively explain the analysis results of the psi index Ψ. We expect that our research results will be widely accepted in the future and will become the foundation for a new research field in science, with a wide range of applications.

1. INTRODUCTION

Research on the so-called "pyramid power" began in the late 1930s [1-4]. However, in general, there are very few systematic academic research papers on pyramid power other than ours, probably because pyramid power has been regarded as having no scientific basis [5-7].

Since October 2007, we have been conducting experiments to detect the pyramid effects on the biosensors using a pyramidal structure (PS). The biosensors were made by evenly cutting cucumber fruits (*Cucumis sativus*). The experiments have been conducted by placing the biosensors at the same time for 30 minutes at the PS apex and the calibration control point 8 m away from the PS, and then measuring the concentration of the volatile components released from the biosensors. As a result of rigorous scientific experiments and analysis, we demonstrated the existence of the potential power of the PS (pyramid power) near the PS apex. We also discovered that when the test subject meditated inside the PS, the PS had the function to convert the test subject's unexplained energy with a time delay. The research results so far have been reported as eleven original papers [8-18], three comprehensive reports [19-21], and one book chapter [22].

The experiments we have been conducting can be divided into the following two main types: (i) an experiment to detect the pyramid effects that appear due to the potential power of the PS (pyramid power) that the PS inherently has; and (ii) an experiment to detect the pyramid effects that appear when a test subject meditates inside the PS. From type (i) experiments, we obtained the following four results so far. 1) The biosensors were placed at the PS apex and the calibration control point 8 m away at the same time for 30 minutes, and then the concentrations of gas released from the biosensors were measured. As a result of calculating the psi index Ψ, which represents the magnitude of the pyramid effects, we obtained statistically significant results. From this, we demonstrated the pyramid effects on the biosensors and the existence of the potential power of the PS. In particular, by analyzing the data from the spring equinox to the autumn equinox, the pyramid effects on the biosensors were significant, $p = 6.0 \times 10^{-3}$ (Welch's t-test, two-tails, the same applies to the p values given hereafter) [14]. 2) We found that the pyramid effects on the biosensors placed in two layers on the PS apex were different between the lower and upper layers, and the pyramid effects on the upper biosensors were always larger than those on the lower biosensors. When comparing the pyramid effects in the lower and upper layers, we obtained $p = 4.0 \times 10^{-7}$, which was statistically highly significant [15]. 3) By analyzing the data for each of the four seasons of winter, spring, summer, and autumn, we found that there were two types of pyramid effects, a seasonally changing pyramid effect and a non-seasonally changing pyramid effect. Comparing the winter and summer data, we obtained $p = 1.8 \times 10^{-3}$, which was a statistically significant result [16]. 4) A phenomenon considered to be entanglement was discovered between the biosensors of the PS apex and the biosensors of the calibration control point. We considered that this phenomenon was occurring, because the biosensors at the PS apex (experimental samples) were affected by the potential power of the PS and they affected the gas production reaction of the biosensors at the calibration control point (control samples) [17, 18]. We have decided to refer to this phenomenon of entanglement between biosensors as the "Bio-Entanglement".

Our purpose of this paper is to show that the pyramid effects on the biosensors can be separated into two, the pyramid effects due to the potential power of the PS and the pyramid effects due to the Bio-Entanglement, and we analyze the characteristics of each pyramid effect.

2. PYRAMIDAL STRUCTURE (PS) AND BIOSENSORS

Figure 1(a) shows the PS used in the experiment. It was a square pyramid with a height of 107 cm, a

ridgeline length of 170 cm and a base length of 188 cm. The tilt angle between the bottom and the side of the PS was 49.1˚ and the base was raised 73 cm from the floor. The frame was made of four aluminum pipes (2 cm diameter, 0.36 cm thick pipe wall), the top ends of which were connected. The four sides of the PS were made of 1 cm thick polystyrene boards. A 0.03 cm thick aluminum plate with a Sierpinski triangle fractal pattern was attached to the four sides of the PS. The four aluminum pipes, polystyrene plates, and fractal-patterned aluminum plates were not grounded. A Faraday cage was installed at the PS apex to electrostatically shield the biosensors and it was connected to the ground. The laboratory was located at 140.1040 degrees east longitude and 35.6399 degrees north latitude.

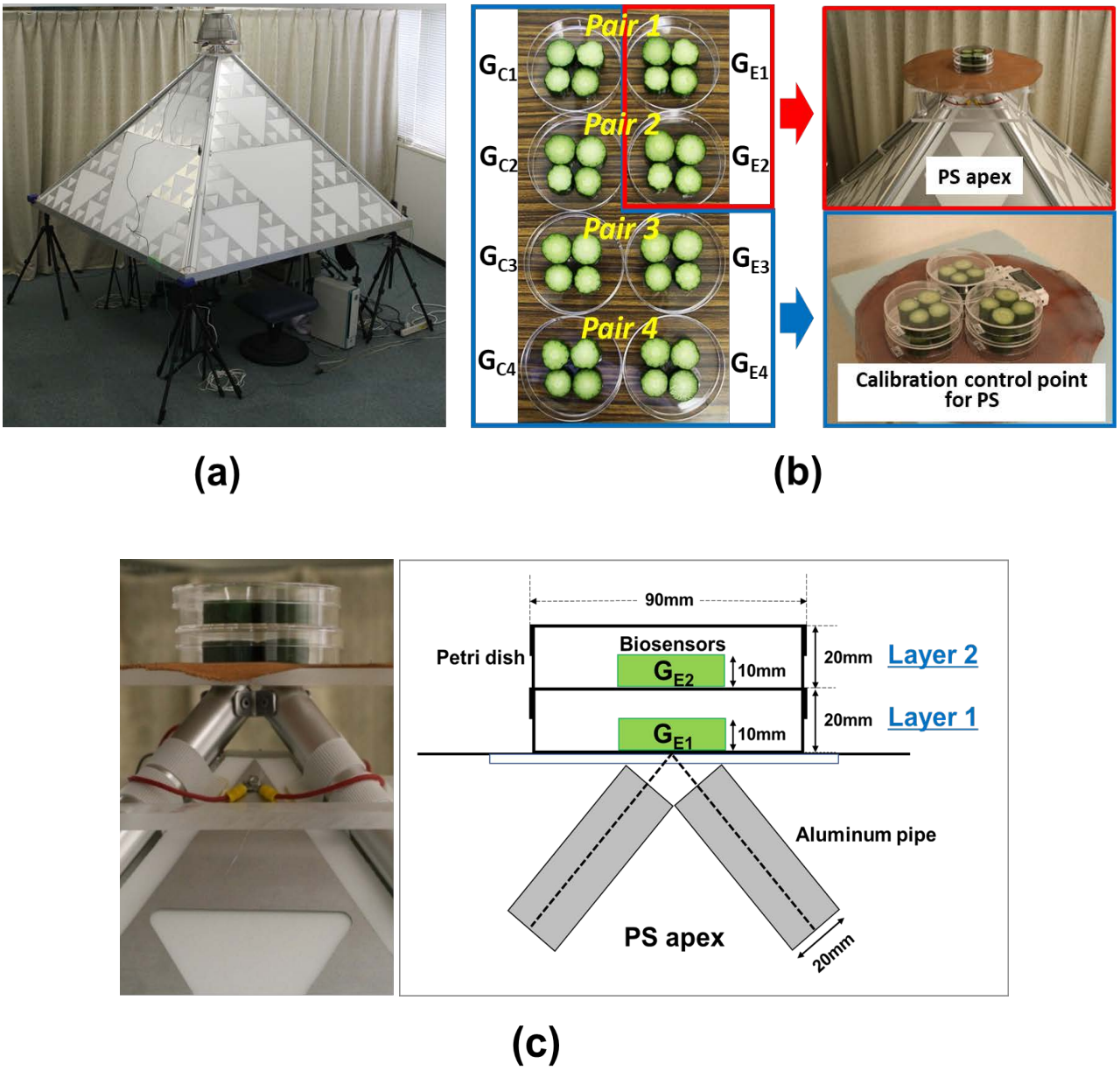

Figure 1. Installation status of the pyramidal structure and the biosensors used in the experiment. (a) The pyramidal structure (PS). (b) left: The biosensors prepared according to SCAT. (b) right: The biosensors placed at the PS apex and calibration control point. (c) left: Photograph of the biosensors at the PS apex. (c) right: Schematic diagram.

The left side of **Figure 1(b)** shows samples used in the simultaneous calibration technique (SCAT) [23]. The SCAT can detect potential power of the PS by using cucumber sections as the biosensors and measuring the concentration of released gas. Thirty-two 1 cm thick sections were cut from four cucumbers and placed in eight Petri dishes, four in each, to prepare four sets of biosensor pairs, namely Pair 1 - Pair 4. Here, G_E was an experimental sample and G_C was a control sample. G_E and G_C had the same cut surface, but with different axial orientations. The direction of the upper surface of the cucumber sections placed on the Petri dish was defined as the direction from the lower surface in contact with the Petri dish to the upper surface. At this time, the upper surface of the sections placed on the G_E was in the same direction as the growth axis of the cucumber. In addition, the upper surface of the section placed on the G_C was in the direction opposite to the growth axis. The growth axis of the cucumber was the direction from the vine side to the flower side of the cucumber fruit. G_{E1}-G_{E4} and G_{C1}-G_{C4} were all considered as uniformly prepared biosensors. However, we reported in a previous paper that the concentrations of gas released due to the characteristics of cucumber differed depending on the direction of the cut surface, and $G_E < G_C$ [12]. In the experiment, G_{E1} and G_{E2} were placed on the PS apex in two layers, and G_{C1}, G_{C2}, G_{E3}, G_{E4}, G_{C3}, and G_{C4} were placed on the calibration control point 8 m away from the PS in two layers (the right side of the **Figure 1(b)**). As shown in **Figure 1(c)**, the difference in height between the two biosensors placed in two layers was 2.0 cm. After placing the biosensors on the PS apex and calibration control point for 30 minutes, we removed the lid of the Petri dish and stored each Petri dish in a closed container with a volume of 2.2 liters. At this time, the closed containers containing the Petri dishes of the pair were stored side by side next to each other. The storage time was 24 - 48 h. After storage, the gas concentration was measured using a gas detector tube and an ethyl acetate detector tube (141 L: Gastech, Japan) and gas sampling pump (GV-100: Gastech). We prepared eight biosensors from four cucumbers in one experimental run, and another experimental run used four new cucumbers to prepare the biosensors. We have used more than 16,000 cucumbers in previous experiments.

3. ANALYSIS OF PSI INDEX Ψ

Figure 2 shows the definition formula of the psi index Ψ, the psi prime index Ψ', the psi double prime index Ψ", and the schematic diagram in which the biosensors are placed. Equations (1)-(5) in **Figure 2** are the psi index Ψ, which has been used as the index of the magnitude of the pyramid effects [14]. To detect the pyramid effects, SCAT is adopted, which can compensate for various factors that affect the concentrations of gas emitted from the cut surface of cucumber. The biosensors G_{E1}-G_{E4} and G_{C1}-G_{C4} are prepared as shown in **Figure 1(b)**.

The magnitude of the pyramid effects in each experiment can be estimated from the non-calibrated psi index Ψ_1 and Ψ_2 in **Figure 2** (1). Next, the magnitude of the pyramid effects calibrated for the variation in the external environment that changes from experiment to experiment can be estimated from the calibrated psi index $\Psi_{1(E\text{-}CAL)}$ and $\Psi_{2(E\text{-}CAL)}$ in **Figure 2** (2). However, even with the calibrated psi index $\Psi_{1(E\text{-}CAL)}$ and $\Psi_{2(E\text{-}CAL)}$, it is not possible to calibrate the difference in steps when the biosensors are placed in two layers. Therefore, in **Figure 2** (4), the psi indexes $\Psi_{1(E\text{-}CAL)Layer1}$ and $\Psi_{2(E\text{-}CAL)Layer2}$ are introduced that can calibrate even the influence of the step. In previous papers, we suggested that Bio-Entanglement between the biosensors might exist [17, 18]. In other words, we found that the influence of the pyramid power on the biosensors G_{E1} and G_{E2} placed at the PS apex affects the emission gas concentration of G_{C1} and G_{C2} placed at the calibration control point of the pair samples of G_{E1} and G_{E2}. From this, it is understood that the calibrated psi indexes $\Psi_{1(E\text{-}CAL)Layer1}$ and $\Psi_{2(E\text{-}CAL)Layer2}$ in **Figure 2** (4) include both the pyramid effects due to the potential power of the PS and the pyramid effects due to the Bio-Entanglement. In **Figure 2**, G_{E1} and G_{E2} affected by the potential power of the PS are shown in red, and G_{C1} and G_{C2} affected by the Bio-Entanglement are shown in blue.

Next, separation of the pyramid effects due to the potential power of the PS and the pyramid effects due to the Bio-Entanglement is considered. The separate results are the psi prime index Ψ' and the psi double prime index Ψ". The psi prime indexes Ψ'_1 and Ψ'_2 in **Figure 2** (6) are the replacements of G_{C1} and

G_{C2} in the non-calibrated psi indexes Ψ_1 and Ψ_2 in Figure 2 (1) with G_{C3} and G_{C4}. In other words, since G_{C1}-G_{C4} is ideally the same biosensor, the pyramid effects are calculated using G_{C3} and G_{C4}, which are not affected by the Bio-Entanglement, instead of G_{C1} and G_{C2}. As a result, the psi prime index $\Psi'_{1(E\text{-}CAL)Layer1}$ and $\Psi'_{2(E\text{-}CAL)Layer2}$ considering the calibration of the layer is represented by Figure 2 (9). In addition, the psi double prime indexes Ψ'', Ψ''_{Layer1} and Ψ''_{Layer2} in Figure 2 (11) show the pyramid effects due to the Bio-Entanglement. These are obtained by subtracting the psi prime index Ψ' from the psi index Ψ. In Figure 2 (4), both the pyramid effects due to the potential power of the PS and the pyramid effects due to the Bio-Entanglement, are included in psi index Ψ. On the other hand, in Figure 2 (9), only the pyramid effects due to the potential power of the PS appears. Also, in Figure 2 (11), only the pyramid effects due to the Bio-Entanglement appears. Therefore, the pyramid effects due to the potential power of the PS and the pyramid effects due to the Bio-Entanglement can be separated.

4. EXPERIMENTAL AND ANALYSIS RESULTS

Using the procedures described in section 3, we clarified that the psi index Ψ, which represents the pyramid effects, includes both the pyramid effects due to the potential power of the PS and the pyramid effects due to the Bio-Entanglement.

Psi index : Ψ

pyramid effect due to
potential power of PS and Bio-Entanglement

$$\Psi_1=100\ln(G_{E1}/G_{C1}),$$
$$\Psi_2=100\ln(G_{E2}/G_{C2}),$$
$$\Psi_3=100\ln(G_{E3}/G_{C3}),$$
$$\Psi_4=100\ln(G_{E4}/G_{C4}). \quad (1)$$
$$\Psi_{1(E\text{-}CAL)}=\Psi_1-(\Psi_3+\Psi_4)/2,$$
$$\Psi_{2(E\text{-}CAL)}=\Psi_2-(\Psi_3+\Psi_4)/2,$$
$$\Psi_{3(E\text{-}CAL)}=\Psi_3-(\Psi_3+\Psi_4)/2,$$
$$\Psi_{4(E\text{-}CAL)}=\Psi_4-(\Psi_3+\Psi_4)/2. \quad (2)$$
$$\Psi_{(E\text{-}CAL)}=(\Psi_{1(E\text{-}CAL)}+\Psi_{2(E\text{-}CAL)})/2. \quad (3)$$
$$\Psi_{1(E\text{-}CAL)Layer1}=\Psi_{1(E\text{-}CAL)}-\Psi_{3(E\text{-}CAL)}$$
$$=\Psi_1-\Psi_3=100\ln(G_{E1}G_{C3}/G_{E3}G_{C1}),$$
$$\Psi_{2(E\text{-}CAL)Layer2}=\Psi_{2(E\text{-}CAL)}-\Psi_{4(E\text{-}CAL)}$$
$$=\Psi_2-\Psi_4=100\ln(G_{E2}G_{C4}/G_{E4}G_{C2}). \quad (4)$$
$$\Psi_{(E\text{-}CAL)LayerAve}=(\Psi_{1(E\text{-}CAL)Layer1}+\Psi_{2(E\text{-}CAL)Layer2})/2$$
$$=\Psi_{(E\text{-}CAL)}. \quad (5)$$

Psi prime index : Ψ'

pyramid effect due to
potential power of PS

$$\Psi'_1=100\ln(G_{E1}/G_{C3}),$$
$$\Psi'_2=100\ln(G_{E2}/G_{C4}),$$
$$\Psi'_3=\Psi_3=100\ln(G_{E3}/G_{C3}),$$
$$\Psi'_4=\Psi_4=100\ln(G_{E4}/G_{C4}). \quad (6)$$
$$\Psi'_{1(E\text{-}CAL)}=\Psi'_1-(\Psi_3+\Psi_4)/2,$$
$$\Psi'_{2(E\text{-}CAL)}=\Psi'_2-(\Psi_3+\Psi_4)/2,$$
$$\Psi'_{3(E\text{-}CAL)}=\Psi'_3-(\Psi_3+\Psi_4)/2,$$
$$\Psi'_{4(E\text{-}CAL)}=\Psi'_4-(\Psi_3+\Psi_4)/2. \quad (7)$$
$$\Psi'_{(E\text{-}CAL)}=(\Psi'_{1(E\text{-}CAL)}+\Psi'_{2(E\text{-}CAL)})/2. \quad (8)$$
$$\Psi'_{1(E\text{-}CAL)Layer1}=\Psi'_{1(E\text{-}CAL)}-\Psi'_{3(E\text{-}CAL)}$$
$$=\Psi'_1-\Psi'_3=100\ln(G_{E1}/G_{E3}),$$
$$\Psi'_{2(E\text{-}CAL)Layer2}=\Psi'_{2(E\text{-}CAL)}-\Psi'_{4(E\text{-}CAL)}$$
$$=\Psi'_2-\Psi'_4=100\ln(G_{E2}/G_{E4}). \quad (9)$$
$$\Psi'_{(E\text{-}CAL)LayerAve}=(\Psi'_{1(E\text{-}CAL)Layer1}+\Psi'_{2(E\text{-}CAL)Layer2})/2$$
$$=\Psi'_{(E\text{-}CAL)}. \quad (10)$$

Psi double prime index : Ψ''

pyramid effect due to
Bio-Entanglement

$$\Psi''_{Layer1}=\Psi_{1(E\text{-}CAL)Layer1}-\Psi'_{1(E\text{-}CAL)Layer1}$$
$$=100\ln(G_{C3}/G_{C1}),$$
$$\Psi''_{Layer2}=\Psi_{2(E\text{-}CAL)Layer2}-\Psi'_{2(E\text{-}CAL)Layer2}$$
$$=100\ln(G_{C4}/G_{C2}). \quad (11)$$
$$\Psi''_{LayerAve}=(\Psi''_{Layer1}+\Psi''_{Layer2})/2. \quad (12)$$

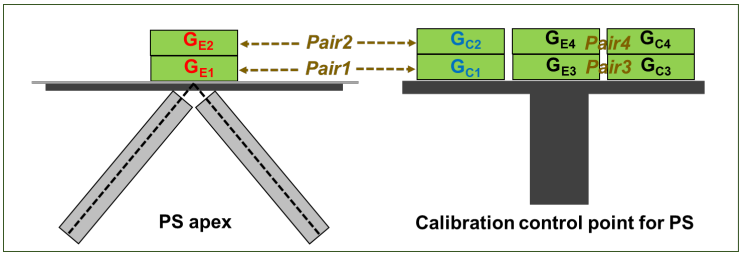

Figure 2. Definition of psi index Ψ, psi prime index Ψ', psi double prime index Ψ'' and the schematic diagram of biosensors of the PS apex and calibration control point. G_{E1} and G_{E2} affected by the potential power of the PS are shown in red, and G_{C1} and G_{C2} affected by the Bio-Entanglement are shown in blue.

Figure 3 shows the seasonal changes of the psi index Ψ (black) which represents the pyramid effects used so far, the psi prime index Ψ'(red) which represents the pyramid effects due to the potential power of the PS, and the psi double prime index Ψ" (blue) which represents the pyramid effects due to the Bio-Entanglement.

Figures 3(a)-(d) show the results of analysis of the data divided into four seasons according to Table 1, respectively. Here, the psi index Ψ shown in black has already been reported in this series of papers III [16]. From the results of Figures 3(a)-(d), the pyramid effects show Layer1 > Layer2 only for the psi double prime index Ψ" in Figure 3(a), and Layer1 < Layer2 for the others. The results of analyzing the presence or absence of a significant difference between Layer1 and Layer2 are shown below in the order of psi index Ψ, psi prime index Ψ', and psi double prime index Ψ". Figure 3(a): $p = 7.6 \times 10^{-2}$, $p = 2.2 \times 10^{-2}$, $p = 6.5 \times 10^{-1}$; Figure 3(b): $p = 1.4 \times 10^{-3}$, $p = 7.5 \times 10^{-3}$, $p = 4.5 \times 10^{-1}$; Figure 3(c): $p = 2.7 \times 10^{-2}$, $p = 5.1 \times 10^{-2}$, $p = 8.4 \times 10^{-1}$; Figure 3(d): $p = 3.6 \times 10^{-3}$, $p = 5.7 \times 10^{-3}$, $p = 5.7 \times 10^{-1}$. We obtained 5% significance for spring in Figure 3(b) and autumn in Figure 3(d) for the psi index Ψ, and no statistically significant difference was detected in other cases. However, as the number of data increases in the future, we expect the psi prime index Ψ' will become significant and Layer1 < Layer2, while we do not expect the psi double prime index Ψ" to detect a significant difference between Layer1 and Layer2 throughout the year.

The seasonal variation of the psi index Ψ in Figure 4(a) has already been reported in this series of papers III [16]. The characteristics of this are that both Layer1 and Layer2 of the psi index Ψ change seasonally, and that Layer1 < Layer2 is satisfied throughout the year. Figure 4(b) shows the seasonal change of psi prime index Ψ' which shows the pyramid effects due to the potential power of the PS. From this result, we can see that Layer1 of the psi prime index Ψ' has hardly changed seasonally. On the other hand, it is possible that Layer2 has seasonal changes that take the maximum value for winter and the minimum value for summer. Also, as in Figure 4(a), the pyramid effects follow the order Layer1 < Layer2 throughout

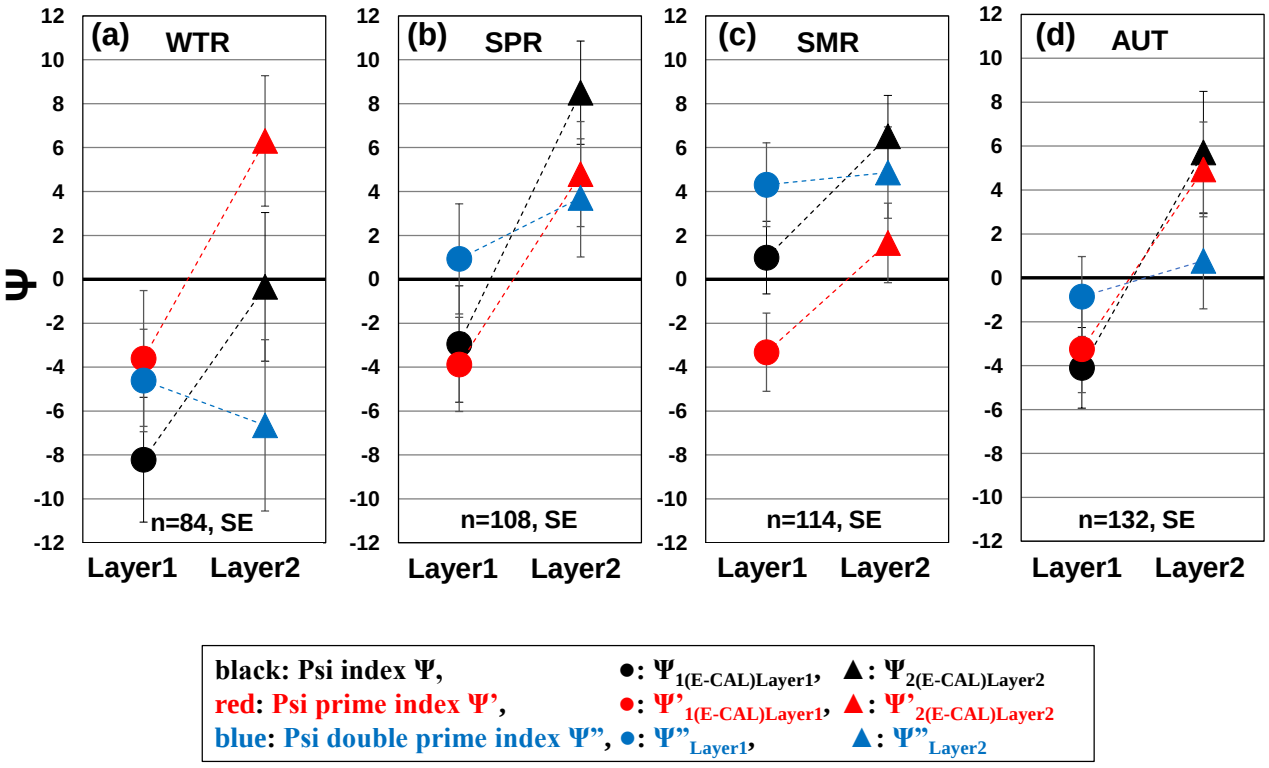

Figure 3. Seasonal changes in Layer1 and Layer2 of psi index Ψ, psi prime index Ψ', psi double prime index Ψ". The error bars are the standard error (SE).

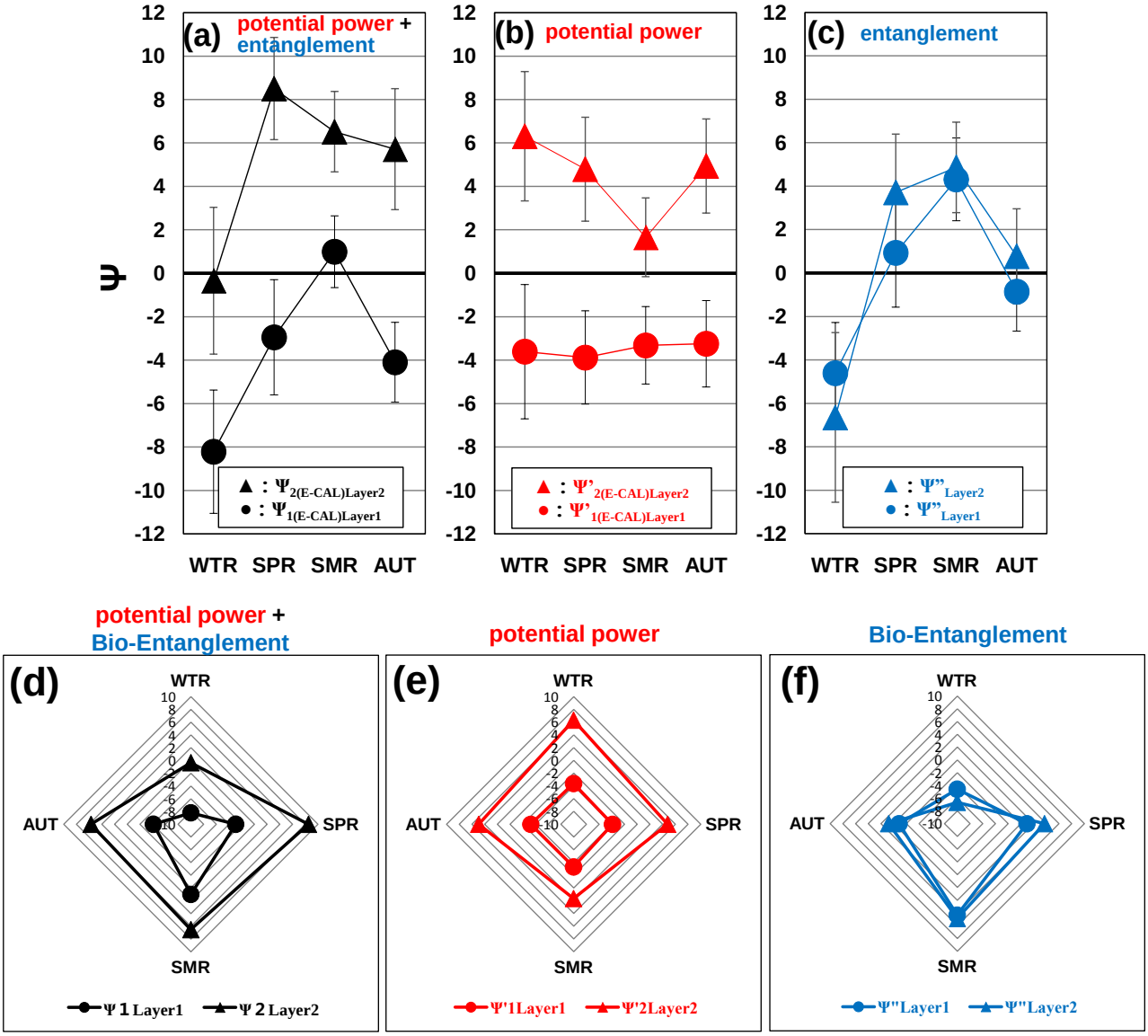

Figure 4. Seasonal changes in psi index Ψ, psi prime index Ψ', psi double prime index Ψ".

Table 1. Seasonal classification and period, and the number of data for each season.

Classification	Season	Period		Number of data
WTR	winter	from the winter solstice to the day before the spring equinox	from 12/22 to 3/20	84
SPR	spring	from the spring equinox to the day before the summer solstice	from 3/21 to 6/20	108
SMR	summer	from the summer solstice to the day before the autumn equinox	from 6/21 to 9/22	144
AUT	autumn	from the autumn equinox to the day before the winter solstice	from 9/23 to 12/21	132

the year. Figure 4(c) shows the seasonal variation of the psi double prime index Ψ" which shows the pyramid effects due to Bio-Entanglement. From this result, we can see that Layer1 and Layer2 of the psi double prime index Ψ" have almost the same seasonal changes, and the values of Layer1 and Layer2 are almost the same throughout the year. From the results of Figure 4(b) and Figure 4(c), the following two results can be considered by reviewing the psi index Ψ in Figure 4(a). 1) The factor why the psi index Ψ is Layer1 < Layer2 throughout the year is mainly due to the potential power of the PS. 2) The factor that causes the psi index Ψ to change seasonally is mainly due to the Bio-Entanglement. Figures 4(d)-(f) are the radar chart representations of Figures 4(a)-(c) with the magnitude of the pyramid effects in the range of −10 to 10. When the shape of the radar chart is a square, the seasonal change is small, and the more it deviates from the square, the larger the seasonal change is.

Figure 5 shows the seasonal variation of the pyramid effects for each layer. Figure 5(a) is the case of Layer1. From this result, we can see that the seasonal change of the psi index Ψ and the psi double prime index Ψ" are qualitatively matched. On the other hand, we can see that the psi prime index Ψ' has almost no seasonal change. Figure 5(b) is the case of Layer2. In this case, similar to the result of Figure 5(a), we can see that the seasonal change of the psi index Ψ and the psi double prime index Ψ" are almost the same. But the change of the psi prime index Ψ' is different qualitatively. Figure 5(c) and Figure 5(d) are the results of Figure 5(a) and Figure 5(b) represented as a radar chart. We can visually understand that the difference between Layer1 and Layer2 is large. Figure 6 shows the changes in the four seasons represented on the radar chart for the psi index Ψ, the psi prime index Ψ', and the psi double prime index Ψ'. This figure allows us to more visually capture the characteristics of the results in Figures 3-5.

5. CONSIDERATION AND MODEL PROPOSAL

We found that the psi index Ψ, which has been used so far to indicate the magnitude of the pyramid effects on the biosensors, includes both the pyramid effects due to the potential power of the PS and the pyramid effects due to Bio-Entanglement. We could discover the Bio-Entanglement by using cucumber sections as sensors without the use of the physical instruments in experiments to detect the pyramid effects. As already reported in this series papers IV and V, the reason why we were able to reveal the existence of Bio-Entanglement is as follows. In the experiment, one of the pair of the biosensors having the same cut surface was placed at the PS apex as the experimental sample, and the other was placed at the calibration control point as a control sample. At this time, the gas generation reaction of the biosensors placed at the calibration control point, which should originally serve as the control, showed an abnormal reaction.

In this report, the effects of the potential power of the PS caused the Bio-Entanglement. On the other hand, two cases have been reported so far that are considered to be similar phenomena. The first case was an experiment to verify the possibility that consciousness of many people may affect the crystallization process of water, and it was reported that abnormal results appeared in the control samples instead of the experimental samples [24]. The second case was an experiment to verify whether the gas concentration from the cucumber sections as the biosensor was affected by the healer's consciousness, and it was reported that the control samples were affected even though the healer's consciousness was focused on the experimental samples [23].

We proposed one model that can explain the characteristics of the pyramid effects due to the potential power of the PS and the pyramid effects due to the Bio-Entanglement.

Figure 7 is a schematic diagram showing the potential power of the PS and the Bio-Entanglement. In a previous paper, in order to explain the pyramid effects on the biosensors, we assumed two types of potential power around the PS apex, and gas generation reactions α and β that respond to each potential power [14]. We also assumed that of the two potential power types, one was distributed near the PS apex and the other was conical from the PS apex [15]. Figure 7(a) shows the model proposed to explain the results of this paper. In this model, the potential power distributed near the PS apex in the previous model is replaced by the Bio-Entanglement, BE. However, the potential power, P extending in a conical shape from

the PS apex still exists. We assumed the effect of potential power P to be greater in Layer2 than in Layer1 (Figure 7(b), Figure 7(c)).

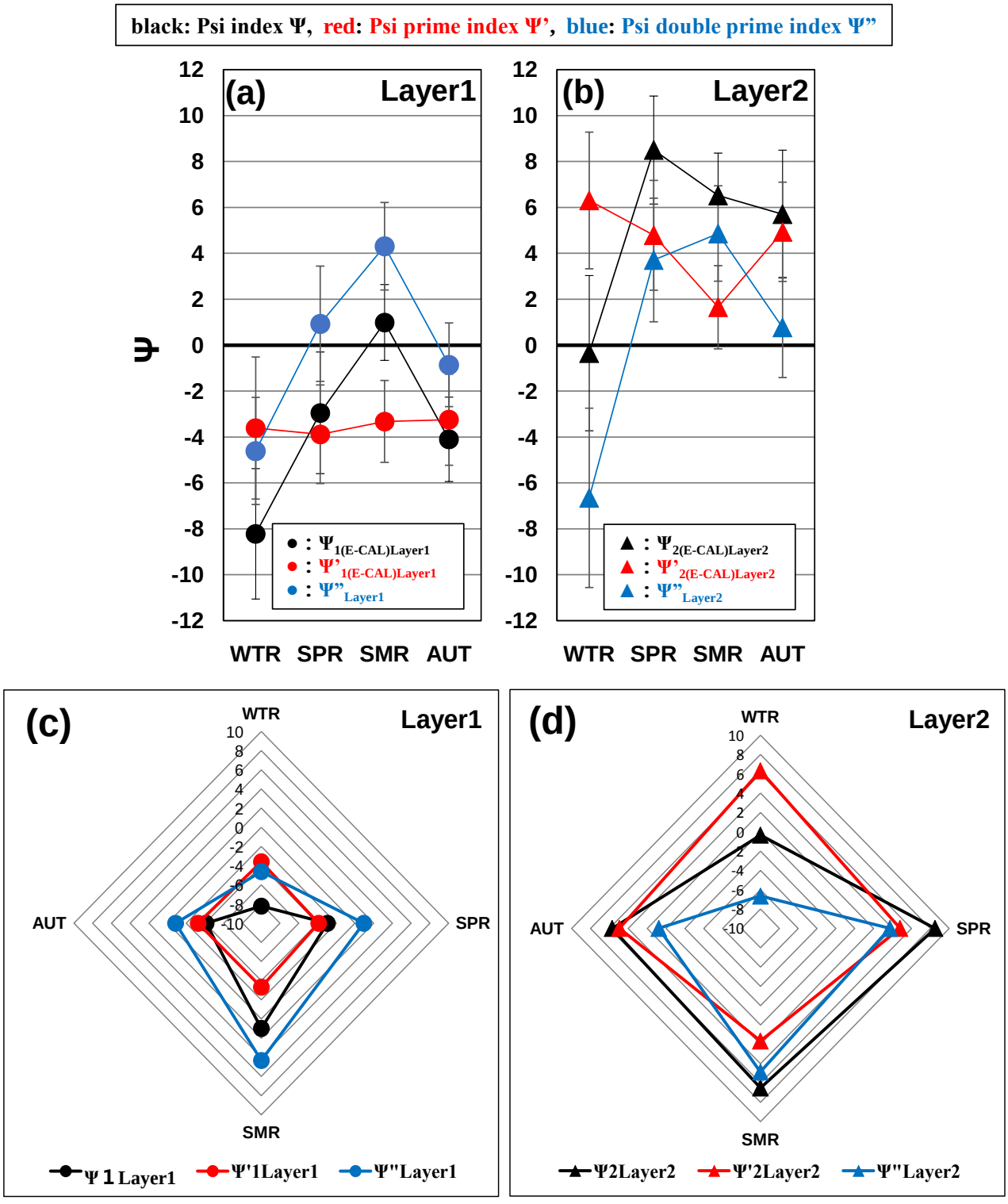

Figure 5. Seasonal changes in psi index Ψ, psi prime index Ψ', psi double prime index Ψ".

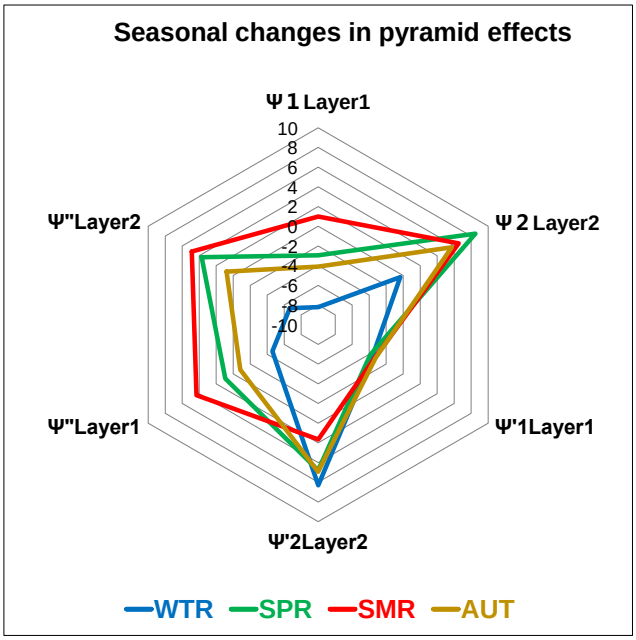

Figure 6. Seasonal changes in psi index Ψ, psi prime index Ψ', psi double prime index Ψ".

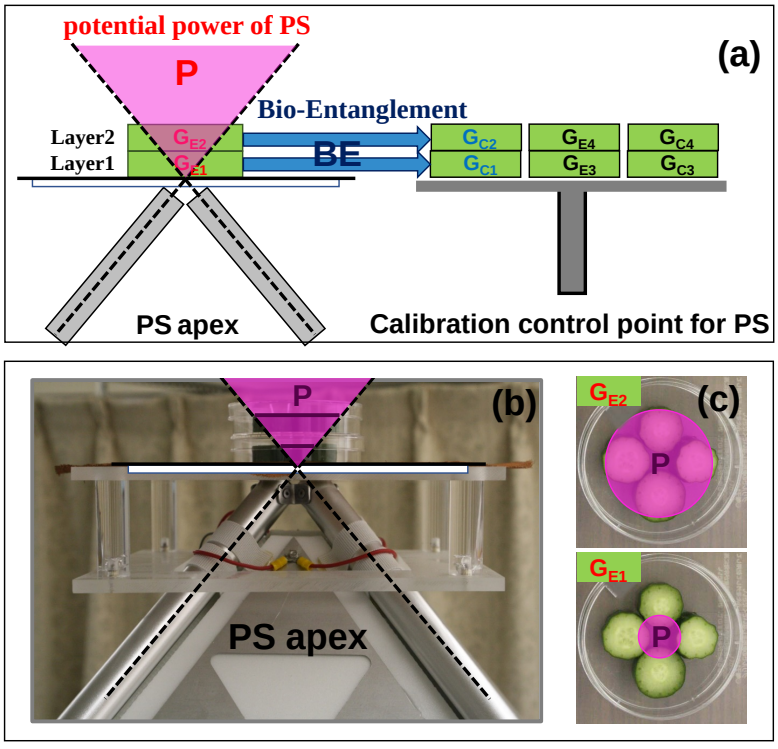

Figure 7. The potential power of the PS and the Bio-Entanglement. (a) Schematic diagram showing the potential power of the PS apex, and the Bio-Entanglement. (b) Image of the potential power near the PS apex. (c) Image of the potential power affecting Layer 1 and Layer 2 on the biosensors placed in two layers at the PS apex.

Figure 8(a) and Figure 8(b) show the respective changes in winter and summer for gas concentration due to the effects of potential power P and Bio-Entanglement BE. In the model proposed this time, we considered only the α reaction as the gas generation reaction. In the previously offered model, we considered two types of gas generation reactions, α and β, because we assumed the potential power of two types of the PS. However, now, we hypothesized that there were two effects on the biosensors, the potential power of the PS and the effects of the Bio-Entanglement, and the Bio-Entanglement was different from the potential power. From this, we judged that there is no problem even if it is assumed that only the α reaction exists as the gas generation reaction. Regarding G_{E1} and G_{E2} at the PS apex, first, for G_{E1} in Layer1, the potential power of the PS was slightly affected in both winter and summer, and the gas concentration increased by G(p). Next, for G_{E2} of Layer2, we assumed that the effect on gas generation was larger in winter than in summer, and WTR G(p) > SMR G(p). For G_{C1} and G_{C2} affected by the Bio-Entanglement BE, we hypothesized that the gas concentration G(BE) was promoted in winter and the gas concentration G(BE) was suppressed in summer. Here, the value of G(BE) did not change between winter and summer. In the model, it was assumed that 1) $\alpha_E < \alpha_C$, which is a characteristic of cucumber; and 2) Layer1 α_E > Layer2 α_E and Layer1 α_C > Layer2 α_C due to the influence of the external environment [12, 15]. By assuming changes in gas concentration as shown in Figure 8, it became possible to qualitatively reproduce the results in Figures 3-6.

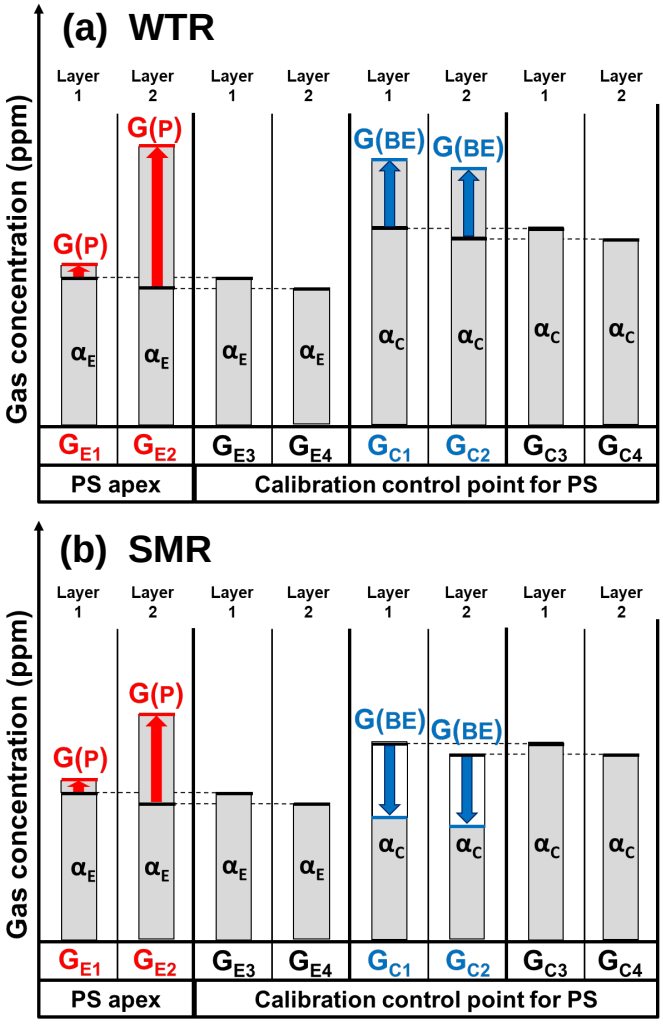

Figure 8. Changes in gas concentration G(P) due to the potential power of the PS and changes in gas concentration G(BE) due to the Bio-Entanglement.

6. CONCLUSION

We reported the phenomenon of the entanglement between biosensors in parts IV and V of the paper series, "Potential Power of the Pyramidal Structure".

In this paper, we found that the pyramid effects due to the potential power of the PS and the pyramid effects due to the Bio-Entanglement were mixed in the psi index Ψ, which is the index showing the magnitude of the pyramid effects. As a result of separating and analyzing each effect, we found that the reason why the pyramid effects on the biosensors at the PS apex are larger in upper layer (Layer2) than in lower layer (Layer1) throughout the year is mainly due to the potential power of the PS. We also found that the factor that causes the pyramid effects to change seasonally is mainly the Bio-Entanglement.

We expect that our research results will be widely accepted in the future and will become the foundation for a new research field in science, with a wide range of applications.

CONFLICTS OF INTEREST

The authors declare no conflicts of interest regarding the publication of this paper.

REFERENCES

1. Sheila, O. and Lynn, S. (1970) Psychic Discoveries behind the Iron Curtain. Prentice-Hall, Inc., Upper Saddle River.
2. Patrick, F. (1973) Pyramid Power: The Millennium Science. Earthpulse Press, Inc., Anchorage.
3. Max, T. and Greg, N. (1974) Pyramid Power. Destiny Books, Rochester.
4. Bill, S. and Ed, P. (1975) The Secret Power of Pyramids. Fawcett Gold Medal, New York.
5. Grandics, P. (2009) The Pyramid Electric Generator. *Infinite Energy*, **84**, 1-4. https://www.researchgate.net/publication/255709759
6. Rubik, B. (2016) Interactions of Pyramidal Structures with Energy and Consciousness. *The Journal of Natural and Social Philosophy*, **12**, 259-275. https://www.researchgate.net/publication/309407219
7. Mikhail, B., Kseniia, V.B., Polina, K. and Andrey, B.E. (2018) Electromagnetic Properties of the Great Pyramid: First Multipole Resonances and Energy Concentration. *Journal of Applied Physics*, **124**, Article ID: 034903. https://doi.org/10.1063/1.5026556
8. Takagi, O., Sakamoto, M., Kokubo, H., Yoichi, H., Kawano, K. and Yamamoto, M. (2013) Meditator's Non-Contact Effect on Cucumbers. *International Journal of Physical Sciences*, **8**, 647-651. https://doi.org/10.5897/IJPS2012.3800
9. Takagi, O., Sakamoto, M., Yoichi, H., Kokubo, H., Kawano, K. and Yamamoto, M. (2015) Discovery of an Anomalous Non-Contact Effect with a Pyramidal Structure. *International Journal of Sciences*, **4**, 42-51. https://doi.org/10.18483/ijSci.714
10. Takagi, O., Sakamoto, M., Yoichi, H., Kokubo, H., Kawano, K. and Yamamoto, M. (2016) An Unknown Force Awakened by a Pyramidal Structure. *International Journal of Sciences*, **5**, 45-56. https://doi.org/10.18483/ijSci.1038
11. Takagi, O., Sakamoto, M., Yoichi, H., Kokubo, H., Kawano, K. and Yamamoto, M. (2018) Discovery of Seasonal Dependence of Bio-Reaction Rhythm with Cucumbers. *International Journal of Science and Research Methodology*, **9**, 163-175. https://www.researchgate.net/publication/331917254
12. Takagi, O., Sakamoto, M., Yoichi, H., Kokubo, H., Kawano, K. and Yamamoto, M. (2018) Relationship between Gas Concentration Emitted from Cut Cucumber Cross Sections and Growth Axis. *International Journal of Science and Research Methodology*, **9**, 153-167. https://www.researchgate.net/publication/331917255
13. Takagi, O., Sakamoto, M., Yoichi, H., Kokubo, H., Kawano, K. and Yamamoto, M. (2019) Discovery of an Un-

explained Long-Distance Effect Caused by the Association between a Pyramidal Structure and Human Unconsciousness. *Journal of International Society of Life Information Science*, **37**, 4-16. https://doi.org/10.18936/islis.37.1_4

14. Takagi, O., Sakamoto, M., Yoichi, H., Kawano, K. and Yamamoto, M. (2019) Potential Power of the Pyramidal Structure. *Natural Science*, **11**, 257-266. https://doi.org/10.4236/ns.2019.118026
15. Takagi, O., Sakamoto, M., Yoichi, H., Kawano, K. and Yamamoto, M. (2020) Potential Power of the Pyramidal Structure II. *Natural Science*, **12**, 248-272. https://doi.org/10.4236/ns.2020.125022
16. Takagi, O., Sakamoto, M., Yoichi, H., Kawano, K. and Yamamoto, M. (2020) Potential Power of the Pyramidal Structure III: Discovery of Pyramid Effects with and without Seasonal Variation. *Natural Science*, **12**, 743-753. https://doi.org/10.4236/ns.2020.1212066
17. Takagi, O., Sakamoto, M., Kawano, K. and Yamamoto, M. (2021) Potential Power of the Pyramidal Structure IV: Discovery of Entanglement Due to Pyramid Effects. *Natural Science*, **13**, 258-272. https://doi.org/10.4236/ns.2021.137022
18. Takagi, O., Sakamoto, M., Kawano, K. and Yamamoto, M. (2021) Potential Power of the Pyramidal Structure V: Seasonal Changes in the Periodicity of Diurnal Variation of Biosensors Caused by Entanglement Due to Pyramid Effects. *Natural Science*, **13**, 523-536. https://doi.org/10.4236/ns.2021.1312046
19. Takagi, O., Sakamoto, M., Yoichi, H., Kokubo, H., Kawano, K. and Yamamoto, M. (2016) Necessary Condition of an Anomalous Phenomenon Discovered by a Pyramidal Structure. *Journal of International Society of Life Information Science*, **34**, 154-157. https://doi.org/10.18936/islis.34.2_154
20. Takagi, O., Sakamoto, M., Yoichi, H., Kokubo, H., Kawano, K. and Yamamoto, M. (2019) Discovery from the Experiment on the Unexplained Functions of the Pyramidal Structure—The Phenomenon Caused by the Personal Relationship. *Journal of International Society of Life Information Science*, **37**, 60-65. https://doi.org/10.18936/islis.37.1_60
21. Takagi, O., Sakamoto, M., Yoichi, H., Kawano, K. and Yamamoto, M. (2020) Scientific Elucidation of Pyramid Power: I. *Journal of International Society of Life Information Science*, **38**, 130-145. https://doi.org/10.18936/islis.38.2_130
22. Takagi, O., Sakamoto, M., Yoichi, H., Kawano, K. and Yamamoto, M. (2020) Chapter 4. Meditator's Non-Contact Effect on Cucumbers. In: Rafatullah, M., Ed., *Theory and Applications of Physical Science*, Vol. 3, Book Publisher International, London, 105-113. https://doi.org/10.9734/bpi/taps/v3
23. Kokubo, H., Takagi, O. and Koyama, S. (2010) Application of a Gas Measurement Method-Measurement of Ki Fields and Non-Contact Healing. *Journal of International Society of Life Information Science*, **28**, 95-103. https://doi.org/10.18936/islis.28.1_95
24. Radin, D., Lund, N., Emoto, M. and Kizu, T. (2008) Effects of Distant Intention on Water Crystal Formation: A Triple-Blind Replication. *Journal of Scientific Exploration*, **22**, 2481-2493. https://www.researchgate.net/publication/255669110